PERGAMON

Journal of Structural Geology 23 (2001) 1327–1335

JOURNAL OF STRUCTURAL GEOLOGY

www.elsevier.com/locate/jstrugeo

Reading history of folding from porphyroblasts

Dazhi Jiang*

Laboratory for Structural Geology and Tectonics, Department of Geology, University of Maryland, College Park, MD 20742, USA

Received 28 April 2000; revised 2 January 2001; accepted 8 January 2001

Abstract

The observation that inclusion trails in porphyroblasts commonly exhibit a more or less constant orientation over a large area, even though the enclosing rocks have been folded, has been considered puzzling by geologists and has generated considerable debate. An analysis of vorticity during multilayer folding in response to layer-parallel shortening shows that the observation is in fact theoretically expected. Folding of multilayers in response to layer-parallel shortening (bulk folding) can be considered kinematically as a time-variable combination of flexural flow and pure shear components. The rotation of a spherical porphyroblast during folding is related to the vorticity history in the vicinity of the porphyroblast by a set of differential equations. For likely folding histories in nature, the solutions to these equations are in agreement with naturally observed patterns. Therefore, it is unnecessary to invoke other mechanisms, such as assuming porphyroblasts to be in 'islands' irrotational with respect to the fold axial plane. More importantly, the theory allows constraints to be placed, from current data sets of porphyroblast inclusion trail geometry, on the history of folding and the competence properties of rocks at the time of folding.

1. Introduction

Over the last two decades, a universal but seemingly puzzling observation emerges from microstructural studies of metamorphic terranes worldwide. It is found that relict foliations (inclusion trails) encapsulated in large rigid minerals (porphyroblasts) like garnets commonly define trajectories that mimic the folds hosting the porphyroblasts, but the trajectories are more gently curved than the hosting folds or are even planar (Fyson, 1980; Bell and Johnson, 1989; Vissers and Mancktelow, 1992; Ilg and Karlstrom, 2000). This observation has led to considerable debate (e.g. Bell et al., 1992; Passchier et al., 1992; Mancktelow and Visser, 1993). Vissers and Mancktelow (1992) and Williams and Jiang (1999) show that the observation can be explained by reasonable end-member fold models or sequential superposition of these end-member models. Williams and Jiang (1999) point out the potential that studies of porphyroblast inclusion trails may provide clues to the deformation paths and the rheological properties of layers in the process of folding. Such information is of paramount importance to geologists (e.g. Hudleston and Lan, 1993, 1995). Here, the variation of vorticity, temporally during fold development and spatially from layer to layer, is considered and the vorticity history is related to porphyroblast rotation. The theory provides a sound explanation for naturally observed porphyroblast inclusion patterns associated with folds and forms the basis for using porphyroblast microstructures to extract folding history and rock rheology information. Only folding of multilayered materials in response to layer-parallel shortening is considered, but more general folding modes can be dealt with following a similar approach.

2. Competence contrasts

During multilayer folding, the layers with different mechanical properties respond to deformation differently and this is described by the concept of competence (Ramsay, 1982; Lister and Williams, 1983; Treagus, 1988; Jiang, 1994). 'Competence' describes the mechanical interaction between different rock units during deformation. It generally does not have a simple mechanical interpretation. In many natural deformations involving layered rocks, such as folding of multilayers with a large fold wavelength compared with the layer thickness, all layers are subjected to approximately the same layer-parallel longitudinal strain rate, and what differs from one layer to another is the layer-parallel shear strain rate (Treagus, 1988, 1997; Price and Cosgrove, 1990; Treagus and Sokoutis, 1992; Jiang, 1994). Based on this observation, a descriptive parameter N, termed the competence factor, was defined by

* Corresponding author. Tel.: +1-301-405-6979, fax: +1-301-314-7970.
E-mail address: dzjiang@geol.umd.edu (D. Jiang).

0191-8141/01/$ - see front matter
PII: S0191-8141(01)00013-X

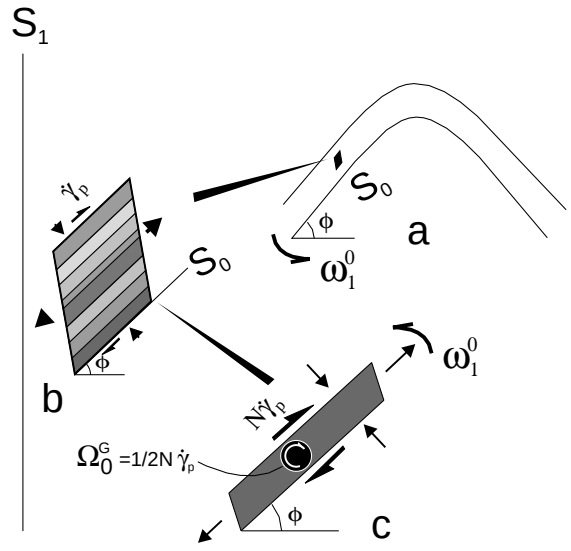

Fig. 1. Flow in a homogeneous domain (b) in the left limb of a normal symmetric fold (a). The bulk shear strain rate $\dot{\gamma}$ imposed by the bulk folding is partitioned differently in the layers (c). S_0 and S_1 are folded layer and axial plane reference frames, respectively. $d\Omega_0/dt$ is the angular velocity of a spherical porphyroblast with respect to S_0. The angular velocity of a porphyroblast relative to S_1, $d\Omega_1/dt$, is equal to $d\Omega_0/dt - d\phi/dt$. N is the competence factor of the layer.

Jiang (1994) as the layer-parallel shear strain rate accommodated in a layer divided by the bulk layer-parallel shear strain rate imposed by the deformation. In other words, N simply expresses the layer-parallel shear strain rate in a given layer as a multiple of the average layer-parallel shear strain rate for the fold limb (Fig. 1). The competence contrast between two layers can be measured by the ratio of their respective competence factors (Jiang, 1994).

3. Vorticity and porphyroblast rotation during multilayer folding

A multilayered system can be regarded as a composite single layer. Kinematically, the folding of such a single layer (bulk folding) at an instant can be viewed as the combination of four end member mechanisms: the flexural flow model (FF), the pure shear model (PS), the tangential longitudinal strain model (TLS), and the slip fold model (SF) (Ramsay, 1967, pp. 292–297; Hobbs et al., 1976, pp. 183–195). The deformation path within an individual layer generally differs from the bulk folding because of partitioning. This phenomenon can be addressed by using the competence factor of the layer. For folding in response to layer-parallel shortening considered here, the SF component is zero because its operation does not accommodate any layer-parallel shortening. The TLS is negligible for multilayer folding (Williams and Jiang, 1999). Therefore, only folding as a combination of FF and PS is considered. In general the combination of FF and PS components will vary from domain to domain. For example the PS component is likely to be relatively stronger in fold hinges than on the limbs unless the folds are isoclinal. This is addressed, at least in part, by the variation of limb dip, e.g. in the hinge the limb dip is close to zero. Two reference frames are used to describe the flow, one fixed to the surface being folded (S_0) and the other fixed to the axial plane (S_1) of the fold. The kinematics of a domain in the left limb of an antiformal fold, as seen in profile, is considered (Fig. 1). Clockwise rotation is taken as positive.

For the end member of folding by PS, folds are produced by passive amplification of pre-existing deflections. The flow is coaxial everywhere and the vorticity with respect to S_1, $\boldsymbol{w}_1$, is zero. The vorticity with respect to S_0, $\boldsymbol{w}_0$, is twice the angular velocity of S_0 with respect to S_1. The angular velocity of the limb (S_0 relative to S_1) resulting from PS is:

$$\left.\frac{d\phi}{dt}\right|_{PS} = -\dot{\epsilon}_{PS}\sin 2\phi \tag{1}$$

The bulk vorticities (written in magnitude throughout the paper) are therefore, respectively:

$$w_1 = 0$$

$$w_0 = 2\left.\frac{d\phi}{dt}\right|_{PS} = -2\dot{\epsilon}_{PS}\sin 2\phi \tag{2}$$

For the end member of folding by FF, the deformation is a layer-parallel simple shear; the imposed layer-parallel shear strain rate is related to the limb angular velocity by (Williams and Jiang, 1999; cf. Ramsay, 1967, pp. 292–297):

$$\dot{\gamma} = \left.\frac{d\phi}{dt}\right|_{FF} \tag{3}$$

The two bulk vorticities are:

$$w_0 = \dot{\gamma}, \qquad w_1 = \dot{\gamma} - 2\left.\frac{d\phi}{dt}\right|_{FF} = -\dot{\gamma} \tag{4}$$

For a given angular velocity of the limb, the amount of shortening normal to S_1 accommodated by FF depends on the shape of the fold (curvature distribution). The two extremes are: a chevron fold (Fig. 2a) where the curvature is localized near a point and the limbs are straight, and a concentric fold (Fig. 2b) where the fold surface, as seen in profile, is circular, i.e. with uniformly distributed curvature. All real folds lie somewhere between these two extremes.

For chevrons, Ramsay and Huber (1987, p. 423) give the stretch ($\lambda^{1/2}$) across the fold as:

$$\lambda^{1/2} = (1 - 2H\phi/W)\cos\phi + 2H\sin\phi/W \tag{5}$$

where, as shown in Fig. 2a, H is the thickness of the folded layer and W is the arc length of the fold wave.

From Eq. (5), the shortening strain rate that is accommodated is:

$$\dot{\epsilon}_{FF} = \frac{d\ln\lambda^{1/2}}{dt} = -\frac{(1-2\phi H/W)\sin\phi}{(1-2\phi H/W)\cos\phi + 2H/W\sin\phi}\left.\frac{d\phi}{dt}\right|_{FF} \quad (6)$$

In the limit of $H/W \rightarrow 0$ (i.e. very thin layer relative to the wavelength), Eq. (6) is reduced to:

$$\dot{\epsilon}_{FF} = -\tan\phi\left.\frac{d\phi}{dt}\right|_{FF} \quad (7)$$

It is sufficient to consider the simpler version (Eq. (7)) only, because the purpose is to use the limiting cases to bracket real folds.

It can be seen from Fig. 2b that as the H-value increases, the hinge area widens until the fold becomes a perfect concentric fold with $W = 2H$ (Fig. 2b). In this case Eq. (5) is reduced to:

$$\lambda^{1/2} = \frac{\sin\phi}{\phi}, \quad (8)$$

(see also Treagus, 1997), and this leads to

$$\dot{\epsilon}_{FF} = \frac{\phi\cos\phi - \sin\phi}{\phi\sin\phi}\left.\frac{d\phi}{dt}\right|_{FF} \quad (9)$$

Combining Eqs. (7) and (9), the angular velocity resulting from FF for a real fold is bracketed by:

$$\left.\frac{d\phi}{dt}\right|_{FF} = \begin{cases} -\dot{\epsilon}_{FF}\cot\phi & \text{chevrons} \\ \dot{\epsilon}_{FF}\dfrac{\phi\sin\phi}{\phi\cos\phi - \sin\phi} & \text{concentric folds} \end{cases} \quad (10)$$

Inserting Eq. (10) into Eq. (4), the two bulk vorticities are:

$$w_0 = \begin{cases} -\dot{\epsilon}_{FF}\cot\phi & \text{chevrons} \\ \dot{\epsilon}_{FF}\dfrac{\phi\sin\phi}{\phi\cos\phi - \sin\phi} & \text{concentric folds} \end{cases} \quad (11a)$$

$$w_1 = \begin{cases} \dot{\epsilon}_{FF}\cot\phi & \text{chevrons} \\ -\dot{\epsilon}_{FF}\dfrac{\phi\sin\phi}{\phi\cos\phi - \sin\phi} & \text{concentric folds} \end{cases} \quad (11b)$$

Natural folding in response to layer-parallel shortening is generally a combination of PS and FF. The partitioning of vorticity into different layers is considered in the following.

Let the total shortening strain rate normal to S_1 at an instant be $\dot{\epsilon}_b$ and let it be accommodated by both PS and FF. We have:

$$\dot{\epsilon}_b = \dot{\epsilon}_{PS} + \dot{\epsilon}_{FF} \quad (12)$$

The angular velocity of the limb, resulting from both PS and FF, is the sum of Eqs. (1) and (10):

$$\frac{d\phi}{dt} = \begin{cases} -\dot{\epsilon}_{PS}\sin 2\phi - \dot{\epsilon}_{FF}\cot\phi & \text{FF component chevrons} \\ -\dot{\epsilon}_{PS}\sin 2\phi - \dot{\epsilon}_{FF}\dfrac{\phi\sin\phi}{\sin\phi - \phi\cos\phi} & \text{FF component concentric folds} \end{cases} \quad (13)$$

By defining $\xi = \dot{\epsilon}_{FF}/\dot{\epsilon}_b$, and therefore $1 - \xi = \dot{\epsilon}_{PS}/\dot{\epsilon}_b$, Eq. (13) becomes:

$$\frac{d\phi}{dt} = \begin{cases} -[(1-\zeta)\sin 2\phi + \zeta\cot\phi]\dot{\epsilon}_b & \text{FF component chevrons} \\ -\left[(1-\zeta)\sin 2\phi + \zeta\dfrac{\phi\sin\phi}{\sin\phi - \phi\cos\phi}\right]\dot{\epsilon}_b & \text{FF component concentric folds} \end{cases} \quad (14)$$

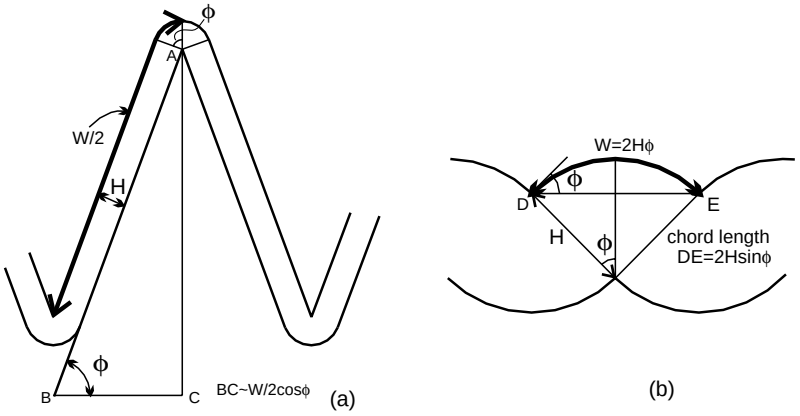

Fig. 2. The distribution of curvature of folds lies between ideal chevron folds (a) and perfect concentric folds (b).

The vorticity with respect to S_0 *in a layer* with competence factor N, w_{L0}, is equal to the sum of Eqs. (2) and (11a) multiplied by N, i.e.:

$$w_{L0} = \begin{cases} -N\dot{\epsilon}_b\left[\xi\cot\phi + 2(1-\xi)\sin2\phi\right] & \text{FF component chevrons} \\ -N\dot{\epsilon}_b\left[\xi\dfrac{\phi\sin\phi}{\sin\phi - \phi\cos\phi} + 2(1-\xi)\sin2\phi\right] & \text{FF component concentric folds} \end{cases} \quad (15)$$

and the vorticity in the layer with respect to S_1 is accordingly:

$$w_{L1} = w_{L0} - 2\frac{d\phi}{dt}\begin{cases} -\dot{\epsilon}_b\left[(N-2)\xi\cot\phi + 2(N-1)(1-\xi)\sin2\phi\right] & \text{FF component chevrons} \\ -\dot{\epsilon}_b\left[(N-2)\xi\dfrac{\phi\sin\phi}{\sin\phi - \phi\cos\phi} + 2(N-1)(1-\xi)\sin2\phi\right] & \text{FF component concentric folds} \end{cases} \quad (16)$$

Eqs. (15) and (16) relate the instantaneous local vorticities in a layer to the bulk folding.

Porphyroblast grain sizes are commonly over an order of magnitude larger than the matrix grain sizes. This means that a porphyroblast can occupy a volume that would contain $\sim 10^3$ matrix grains. It is reasonable to assume that the vorticity the porphyroblast accommodates is the averaged matrix vorticity (averaged over $\sim 10^3$ matrix grains) (cf. Williams and Jiang, 1999). The relationship from continuum mechanics that the angular velocity of a spherical rigid inclusion is equal to half the matrix vorticity (e.g. McKenzie and Jackson, 1983; Triton, 1988, p. 82) is therefore justifiably adopted. Using Ω_0 and Ω_1 to denote finite rotation of porphyroblasts with respect to S_0 and S_1, respectively, ($d\Omega_0/dt$ and $d\Omega_1/dt$ are the corresponding angular velocities), Eqs. (15) and (16) lead to:

$$\frac{d\Omega_0}{dt} = \begin{cases} -0.5N\dot{\epsilon}_b\left[\xi\cot\phi + 2(1-\xi)\sin2\phi\right] & \text{FF component chevrons} \\ -0.5N\dot{\epsilon}_b\left[\xi\dfrac{\phi\sin\phi}{\sin\phi - \phi\cos\phi} + 2(1-\xi)\sin2\phi\right] & \text{FF component concentric folds} \end{cases} \quad (17)$$

and

$$\frac{d\Omega_1}{dt} = \begin{cases} -0.5\dot{\epsilon}_b\left[(N-2)\xi\cot\phi + 2(N-1)(1-\xi)\sin2\phi\right] & \text{FF component chevrons} \\ -0.5\dot{\epsilon}_b\left[(N-2)\xi\dfrac{\phi\sin\phi}{\sin\phi - \phi\cos\phi} + 2(N-1)(1-\xi)\sin2\phi\right] & \text{FF component concentric folds} \end{cases} \quad (18)$$

Using Eq. (14) to eliminate $\dot{\epsilon}_b$ from Eqs. (17) and (18), we obtain the following important differential equations describing the rotation of spherical porphyroblasts during folding:

$$\frac{d\Omega_0}{d\phi} = \frac{N\left[0.5\xi\cot\phi + (1-\xi)\sin2\phi\right]}{\xi\cot\phi + (1-\xi)\sin2\phi} \quad (19a)$$

FF component chevrons

$$\frac{d\Omega_0}{d\phi} = \frac{N\left[0.5\xi\dfrac{\phi\sin\phi}{\sin\phi - \phi\cos\phi} + (1-\xi)\sin2\phi\right]}{\xi\dfrac{\phi\sin\phi}{\sin\phi - \phi\cos\phi} + (1-\xi)\sin2\phi} \quad (19b)$$

FF component concentric folds

$$\frac{d\Omega_1}{d\phi} = \frac{N\left[0.5\xi\cot\phi + (1-\xi)\sin2\phi\right]}{\xi\cot\phi + (1-\xi)\sin2\phi} - 1 \quad (20a)$$

FF component chevrons

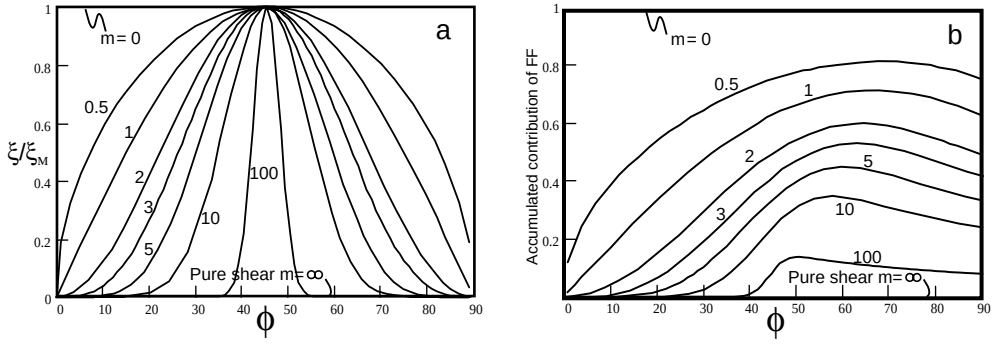

Fig. 3. (a) Instantaneous FF component (ξ), normalized against ξ_M, as a function of ϕ; (in degrees) for various m values. (b) The accumulated contribution of FF to folding as a function of ϕ for different m values. $m = 0$ and $m = \infty$ correspond to 100% FF and 100% PS, respectively. See text for details.

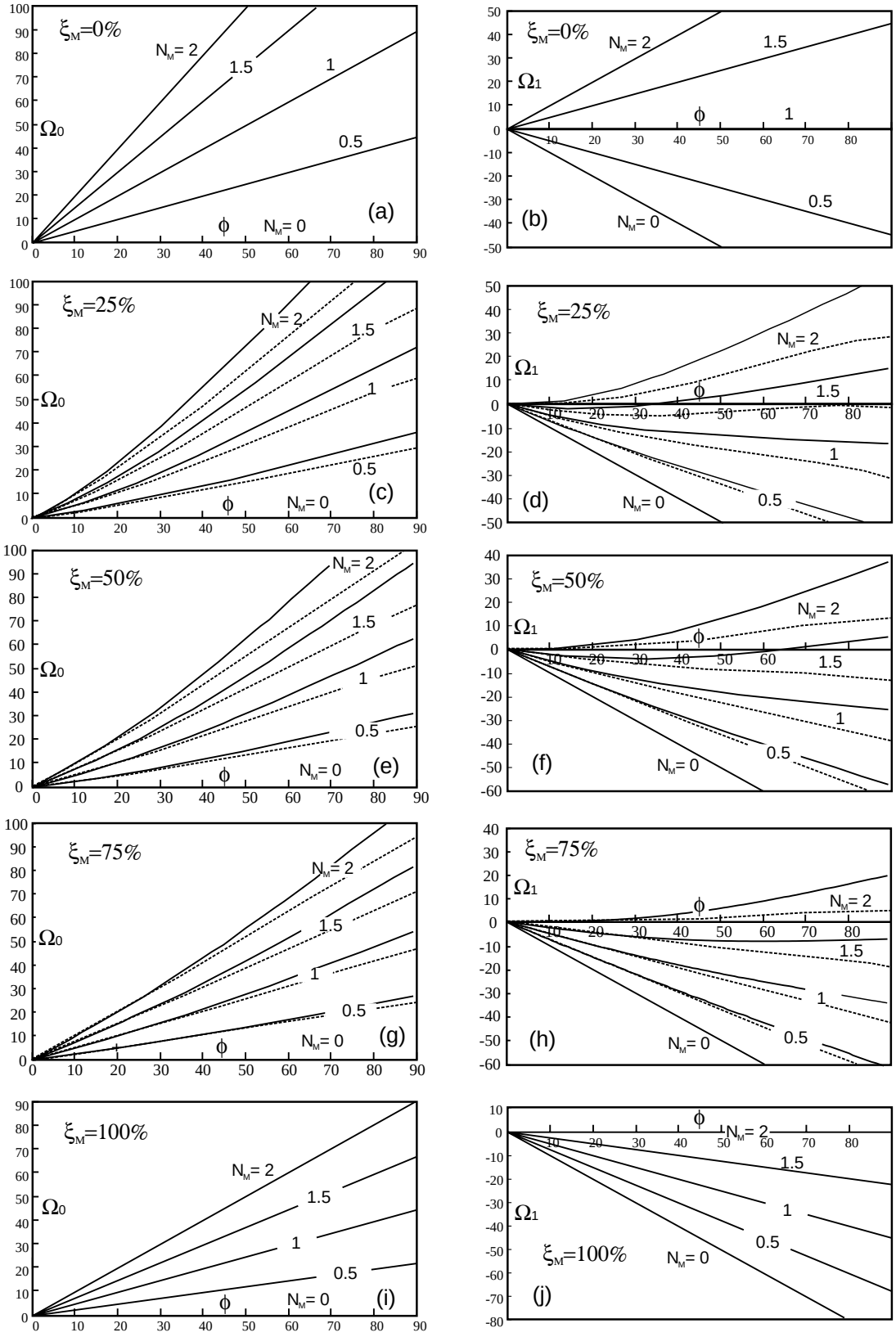

Fig. 4. Variation in finite rotations Ω_0 and Ω_1 (in degrees) with limb dip ϕ (in degrees) for constant ξ and N histories. A solid line represents the case for which the FF component corresponds to an ideal chevron fold and a dashed line represents the case for which the FF component corresponds to an ideal concentric fold.

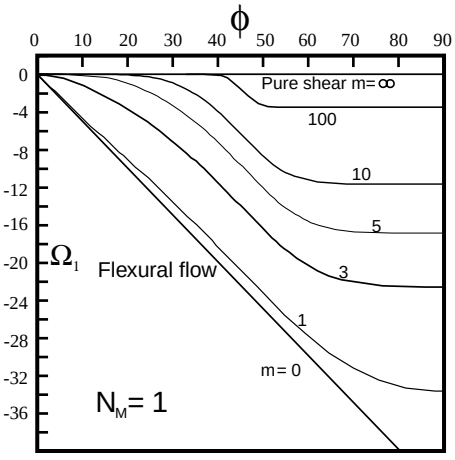

Fig. 5. Finite rotation Ω_1 (in degrees) as a function of ϕ (in degrees) when there is no partitioning. The FF component is assumed to be that for ideal chevron folds.

$$\frac{d\Omega_1}{d\phi} = \frac{N\left[0.5\xi\frac{\phi\sin\phi}{\sin\phi - \phi\cos\phi} + (1-\xi)\sin 2\phi\right]}{\xi\frac{\phi\sin\phi}{\sin\phi - \phi\cos\phi} + (1-\xi)\sin 2\phi} - 1 \tag{20b}$$

FF component concentric folds

For any given history of bulk folding (ξ–ϕ history) and given competence factor history (N–ϕ history), Eqs. (19) and (20) can be solved numerically to predict the history of porphyroblast rotation. Let us now consider solutions to these equations for likely natural folding histories.

4. Solutions and discussion

Out of the vast number of works on the mechanics of folding (see reviews in Chapple, 1969; Ghosh, 1993, p. 273; Treagus, 1997) emerges the following three-stage picture of the bulk folding path: in the early stage of folding before the end of wavelength selection, layer-parallel homogeneous shortening (PS) dominates (ξ close to zero) and the partitioning of flow is insignificant (N close to one). Then active buckling follows and the folding has a significant component of FF (high ξ) and the flow is significantly partitioned in different layers (greater deviation of N's from one). Finally, as limb dip increases, 'flattening' (PS) becomes more important, and the bulk PS is partitioned in different layers (Ghosh, 1993, p. 273; Treagus, 1997). From a theoretical point of view, this general three-stage picture can be conveniently approximated by the following functions: $\xi(\phi) = \xi_M \sin^m(2\phi)$ and $N(\phi) = 1 + (N_M - 1)\sin^n(2\phi)$, where ξ_M (≤ 1) is the maximum value of ξ reached during folding and N_M (≥ 0) is the extremum of N reached during folding. The exponents m and n (both ≥ 0) measure the gradient of the variation of ξ and N, respectively. The higher the value of m (or n) the narrower the range in which ξ (or N) is close to ξ_M (or N_M). $m = 0$ represents a constant ξ ($= \xi_M$) history, and if $\xi_M = 1$ as well, the folding is 100% FF. $m \to \infty$ represents 100% PS (Fig. 3a). It is readily seen that at $\phi = 0°$, $\xi = 0$ (100% PS) and $N = 1$ (no partitioning). ξ increases as ϕ increases and reaches the maximum value ξ_M (≤ 1) at $\phi = 45°$. It then decreases as ϕ approaches 90° (Fig. 3a). The N-value of a layer starts at one when $\phi = 0°$. It deviates progressively from one as ϕ increases from 0 to 45° where it reaches its extremum and then gradually returns to one as ϕ approaches 90°. Structural geologists tend to consider the sequential superposition of FF and PS (Ramsay, 1967, pp. 411–415; Vissers and Mancktelow, 1992; Williams and Jiang, 1999). However, both FF and PS components are more likely to operate throughout the folding history, with their relative significance varying with limb dip. In this case, the accumulated contribution of FF to folding up to a limb dip ϕ is best measured by the average of ξ over ϕ, which for the theoretical considerations of this paper is (Fig. 3b):

$$\bar{\xi}(\phi) = \frac{1}{\phi}\xi_M \int_0^{\phi} \sin^m(2\phi)d\phi,$$

Fig. 4 plots solutions to Eqs. (19) and (20) when $m = 0$ and $n = 0$, i.e. constant N and ξ histories. Fig. 5 plots solutions to Eq. (20a) for the case of no partitioning ($N_M = 1$, in which case $N \equiv 1$ and is independent of n) and $\xi_M = 1$. Fig. 6 plots solutions to Eq. (20a) for $\xi_M = 1$ and various N_M, m and n values.

When there is no partitioning (Fig. 5), porphyroblast rotates in the same sense as the limb ($\Omega_1 < 0$ for the left limb, Fig. 1) but the rotation is less than the limb dip ($|\Omega_1| < \phi$). Therefore, inclusion trails in such porphyroblasts from two adjacent limbs will define a fold that is a subdued form of the hosting fold (Fig. 7a). For end-member FF ($m = 0$), the maximum rotation is 45° when the hosting fold is isoclinal ($\phi = 90°$). The amount of rotation decreases as m increases (more PS component), and when the folding is 100% PS ($m = \infty$), the rotation is zero, and the inclusion tails are planar throughout the folding history (Figs. 5 and 7b). When there is partitioning (Fig. 6), porphyroblast rotation has the same sense as the limb for $0 \leq N_M < 1$, i.e. relatively competent layers (Jiang, 1994) (Fig. 6a–c). The maximum rotation is $|\Omega_1| = \phi$, realized when $n = 0$ and the layer is folded by TLS mechanism ($N_M = 0$ curve in Fig. 4b, d, f, h and j). As n increases, $|\Omega_1| < \phi$ and the amount of rotation decreases (Fig. 6a–c). For $N_M > 1$, i.e. relatively incompetent layers (Jiang, 1994), if $n = 0$ porphyroblast rotation has the same sense as the limb ($\Omega_1 < 0$) for pure FF folding for N_M up to two (Fig. 4j). Higher N_M generally means $\Omega_1 > 0$, and the higher N_M and/or the more PS component, the more likely is $\Omega_1 > 0$ ($N_M > 1$ curves in Fig. 4b, $N_M \sim 2$ curves in Fig. 4d, f and h). For $N_M = 2$ (Fig. 6d–f), the sense of porphyroblast rotation is the

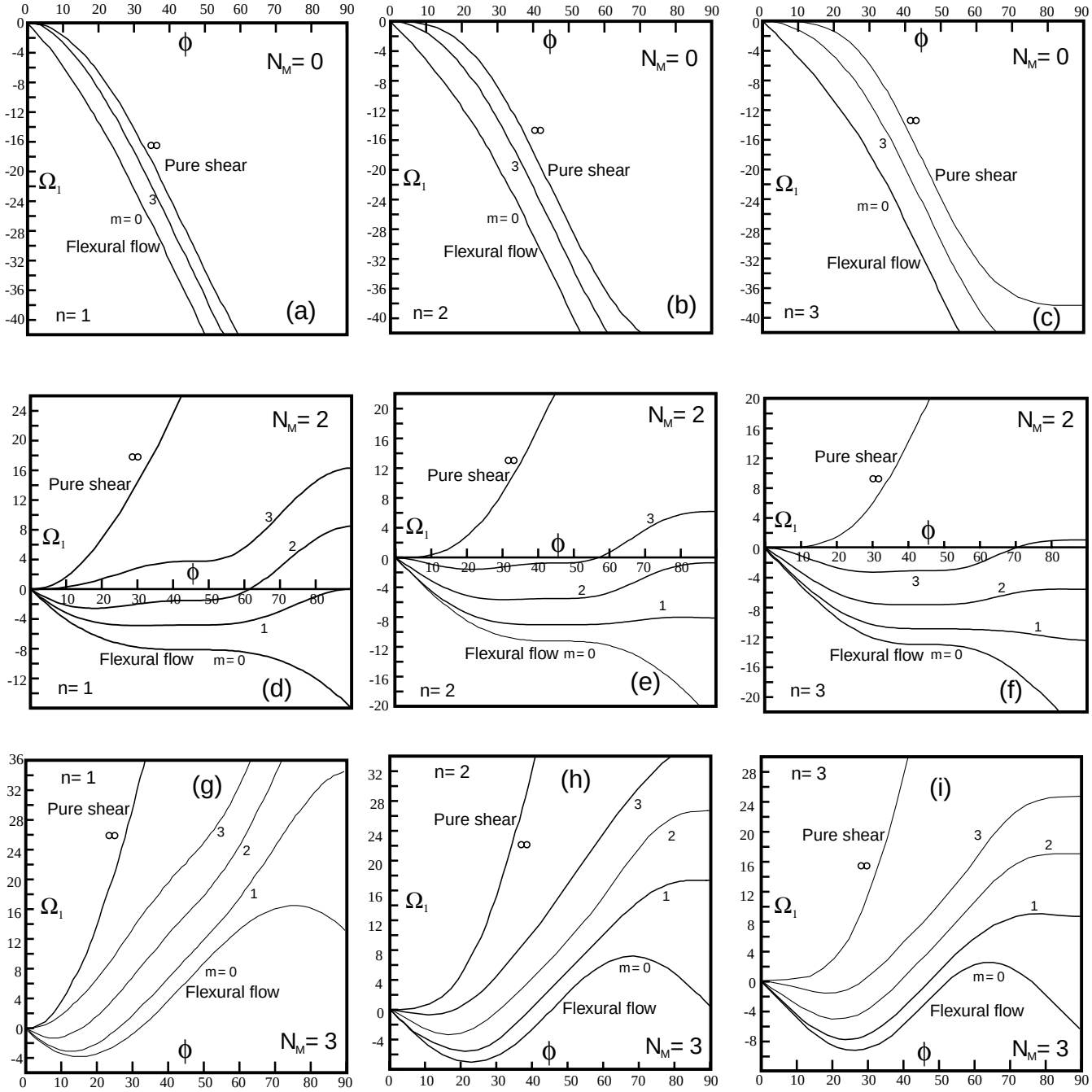

Fig. 6. Variation in finite rotation Ω_1 (in degrees) with limb dip ϕ (in degrees) for various m and n values when there is partitioning. The FF component is assumed to be ideally chevron. See text for details.

same as the limb ($\Omega_1 < 0$) for ϕ up to 60°, for $m < 2$ at $n = 1$, $m < 3$ at $n = 2$, and $m \leq 3$ at $n = 3$. When $N_M > 2$ (Fig. 6g–i), generally $\Omega_1 > 0$. $\Omega_1 > 0$ means inverse curvature of inclusion trails (i.e. a synform defined by inclusion trails in an antiform host fold, Fig. 7c), which is only rarely observed in natural rocks (P.F. Williams and P. Stringer, 1998, pers. commmun.).

As far as I am aware, the current data set of porphyroblast inclusion microstructures all come from relatively incompetent layers, usually layers with a strong layer-parallel anisotropy prior to folding. It is easy to imagine that these layers would accommodate higher layer-parallel shear strain rates than does the multilayer as a whole. Therefore these layers are generally expected to have their N_M-values ≥ 1. This, together with the fact that $\Omega_1 > 0$ (Fig. 7c) is rarely observed in nature and that constant N histories are unlikely, suggests that Figs. 5 and 6d–f are most relevant to natural folding in metamorphic rocks. Overall, the current data set is most compatible with the following range of parameters: $1 \leq N_M \leq 2$, $m \leq 3$ and

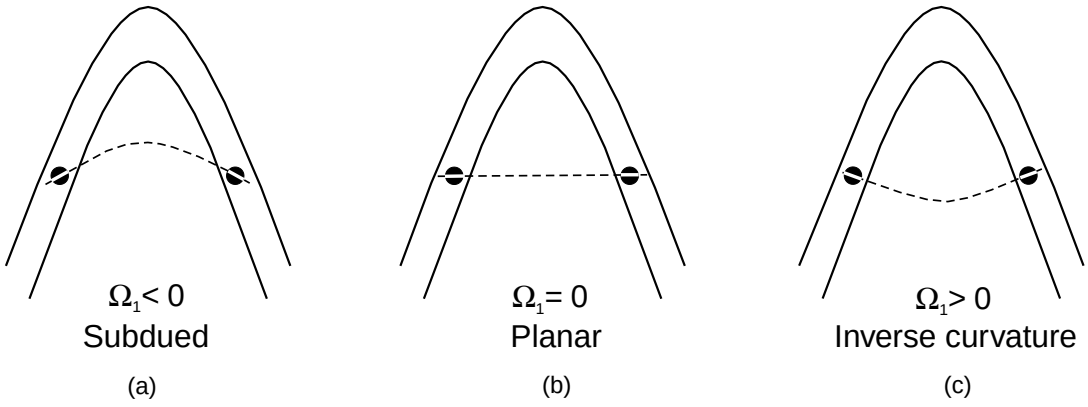

Fig. 7. Porphyroblast (black solid circle) inclusion trails across two adjacent fold limbs may define a trajectory that is a subdued form (a) of the hosting fold, a planar surface (b), or inversely curved (c), depending on the amount and sense of porphyroblast rotation with respect to the axial plane of the hosting fold.

$n \geq 2$ (Figs. 5 and 6e and f). This implies that the maximum competence factor of a layer under metamorphic conditions is probably near two (note the difference between competence factor and competence contrast, the latter being the ratio of two competence factors). Folding involves a considerable FF component (m between zero and three in order for $\Omega_1 \leq 0$). Strong partitioning ($N \sim 2$) is concentrated near $\phi = 45°$ ($n \geq 2$). A higher m-value (more PS) requires a correspondingly higher n-value (narrower ϕ range in which there is strong partitioning) in order for $\Omega_1 \leq 0$. For all these cases, the rotation of porphyroblasts with respect to the axial plane is small, generally $\ll 45°$. Therefore, the natural observation that porphyroblasts appear to have rotated little across the hosting fold limbs is compatible with theoretical predictions. It is unnecessary to invoke other mechanisms such as assuming porphyroblasts to be in 'islands' irrotational relative to S_1 and the folding of a slip fold mechanism (Bell and Johnson, 1989).

5. Conclusions

Folding of multilayers in response to layer-parallel shortening can be described by a time-variable combination of flexural flow and pure shear components. Such folding generally leads to partitioning of vorticity in different layers. The vorticity history in a layer is responsible for the finite rotation of spherical porphyroblasts contained in that layer.

For realistic folding histories, theoretically-predicted finite rotation of spherical porphyroblasts is compatible with naturally observed geometries of porphyroblast inclusion trails associated with folds. It is unnecessary to invoke any other mechanisms. If there is no partitioning, inclusion trails always define subdued folds. The more the PS component, the more subdued are the inclusion trail folds. If there is partitioning, the rotation of porphyroblasts is a result of the interplay among the layer competence factor, bulk folding history, and the history of partitioning.

The theory presented in this paper, together with the current data set of porphyroblast inclusion geometries, allows some constraints to be placed on natural folding under metamorphic conditions. It appears that the maximum competence factor (as defined in Jiang, 1994) for a layer under metamorphic conditions is around two. Where there are competence contrasts, folding has a significant FF component (m between zero and three, Fig. 3). During folding, the strongest partitioning occurs for around 45° ($n \geq 2$). For all these cases, porphyroblast inclusion trails define subdued folds or are planar (Fig. 7a and b), and there is little rotation of porphyroblasts with respect to the axial plane, generally $\ll 45°$. The theory therefore provides a basis for reading the history of folding and the competence properties of rocks at the time of folding from porphyroblast microstructural data.

The theory is only applicable to nearly spherical porphyroblasts. Most garnets associated with folds approximate spherical shapes. The rotation of non-spherical porphyroblasts is related to both vorticity and stretching. A theory describing their rotation during multilayer folding is being developed.

Acknowledgements

I thank Dr. Paul Williams and Dr. Peter Stringer for inspiring discussion and two anonymous reviewers for constructive comments.

References

Bell, T.H., Johnson, S.E., 1989. Porphyroblast inclusion trails: the key to orogenesis. Journal of Metamorphic Geology 7, 279–310.

Bell, T.H., Johnson, S.E., Davis, B., Forde, A., Hayward, N., Wilkins, C., 1992. Porphyroblast inclusion-trail orientation data: eppure non son girate!. Journal of Metamorphic Geology 10, 295–307.

Chapple, W.M., 1969. Fold shape and rheology: the folding of an isolated viscous-plastic layer. Tectonophysics 7, 97–116.

Fyson, W.K., 1980. Fold fabrics and emplacement of an Archean granitoid

pluton, Cleft Lake, Northwest Territories. Canadian Journal of Earth Sciences 17, 325–332.

Ghosh, S.K., 1993. Structural Geology. Fundamentals and Modern Developments. Pergamon Press, Oxford.

Hobbs, B.E., Means, W.D., Williams, P.F., 1976. An Outline of Structural Geology. John Wiley, New York.

Hudleston, P.J., Lan, L., 1993. Information from fold shapes. Journal of Structural Geology 15, 253–264.

Hudleston, P.J., Lan, L., 1995. Rheological information from geological structures. Pure and Applied Geophysics 145, 605–620.

Ilg, B.R., Karlstrom, K.E., 2000. Porphyroblast inclusion trail geometries in the Grand Canyon: evidence for non-rotation or rotation? Journal of Structural Geology 22, 231–243.

Jiang, D., 1994. Flow variation in layered rocks subjected to bulk flow of various kinematic vorticities: theory and geological implications. Journal of Structural Geology 16, 1159–1172.

Lister, G.S., Williams, P.F., 1983. The partitioning of deformation in flowing rock masses. Tectonophysics 92, 1–33.

Mancktelow, N.S., Visser, P., 1993. The rotation of garnet porphyroblasts around a single fold, Lukmanier Pass, Central Alps: reply. Journal of Structural Geology 15, 1369–1372.

McKenzie, D., Jackson, J., 1983. The relationship between strain rates, crustal thickening, palaeomagnetism, finite strain and fault movements within a deformation zone. Earth and Planetary Science Letters 65, 182–202.

Passchier, C.W., Trouw, R.A.J., Zwart, H.J., Vissers, R.L.M., 1992. Porphyroblast rotation: eppur si muove? Journal of Metamorphic Geology 10, 283–294.

Price, N.J., Cosgrove, J.W., 1990. Analysis of Geological Structures. Cambridge University Press, Cambridge.

Ramsay, J.G., 1967. Folding and Fracturing of Rocks. McGraw-Hill, New York.

Ramsay, J.G., 1982. Rock ductility and its influence on the development of tectonic structures in mountain belts. In: Hsü, K.J. (Ed.). Mountain Building Processes. Academic Press, London, pp. 111–127.

Ramsay, J.G., Huber, M.I., 1987. The Techniques of Modern Structural Geology, Vol. 2. Folds and Fractures. Academic Press, London.

Treagus, S.H., 1988. Strain refraction in layered systems. Journal of Structural Geology 10, 517–527.

Treagus, S.H., 1997. Modelling deformation partitioning in folds. In: Sengupta, S. (Ed.). Evolution of Geological Structures in Micro- to Macro-scales. Chapman & Hall, London, pp. 341–372.

Treagus, S.H., Sokoutis, D., 1992. Laboratory modelling of strain variation across rheological boundaries. Journal of Structural Geology 14, 405–424.

Triton, D.J., 1988. Physical fluid dynamics. Journal of Structural Geology Clarendon Press, Oxford.

Vissers, P., Mancktelow, N.S., 1992. The rotation of garnet porphyroblasts around a single fold, Lukmanier Pass, Central Alps. Journal of Structural Geology 14, 1193–1202.

Williams, P.F., Jiang, D., 1999. Rotating garnet. Journal of Metamorphic Geology 17, 367–378.